Inorg. Chem. **2004**, *43*, 7636–7647

Why Is Re–Re Bond Formation/Cleavage in $[Re(bpy)(CO)_3]_2$ Different from That in $[Re(CO)_5]_2$? Experimental and Theoretical Studies on the Dimers and Fragments

Etsuko Fujita* and James T. Muckerman*

Chemistry Department, Brookhaven National Laboratory, Upton, New York 11973-5000

Received August 9, 2004

The $Re(NN)(CO)_3(THF)$ (NN = bpy = 2,2′-bipyridine or dmb = 4,4′-dimethyl-2,2′-bipyridine) radical, produced by homolysis of $[Re(NN)(CO)_3]_2$ in THF solution by visible irradiation, dimerizes with rate constants $k_d = 20 \pm 3$ and 11 ± 4 M^{-1} s^{-1} for NN = dmb and bpy, respectively. The dimerization processes are strikingly slow compared to those of typical metal radicals including $Re(CO)_5$ ($k_d \approx 10^9$ M^{-1} s^{-1}). In order to explain such slow reactions, we have performed B3LYP hybrid DFT and fully ab initio RHF and MP2 calculations on several conformations of $[Re(bpy)(CO)_3]_2$ (*cis*, *trans*, skewed *cis*, skewed *trans*) and $[Re(CO)_5]_2$ (staggered) and on their constituent monomer radicals and anions. The calculations show that the most stable geometry of $[Re(bpy)(CO)_3]_2$ is skewed *cis*, and the experimental infrared spectrum and photochemical properties of the $[Re(bpy)(CO)_3]_2$ dimer are best described by the calculated properties of the skewed *cis* conformer in which there is no low-lying unoccupied orbital that is predominantly σ_{MM}* in character. The $Re(bpy)(CO)_3(THF)$ ligand radical is more stable than the 5-coordinate "17-electron" metal radical, $Re(bpy)(CO)_3$, suggesting that the extremely slow dimerization rate most likely arises from the solvent blocking the binding site (i.e., the estimated fraction of the five-coordinate monomer is 1.6×10^{-2}). Theoretical results are consistent with our experimental results that the dimerization process proceeds via the Re centered radical, which is involved in a pre-equilibrium favoring the ligand-centered radical. Furthermore, time-dependent DFT calculations on $[Re(bpy)(CO)_3]_2$ and $[Re(bpy)(CO)_3]^-$ identify the origin of UV–vis absorption in THF.

Introduction

Photochemical homolysis of carbonyl-containing metal–metal bonded dimers has been extensively studied and has become a well-known route to formation of reactive metal-centered radicals as intermediates in organometallic chemistry.[1−3] The geometrical structure,[4,5] infrared spectroscopy,[6−8] molecular beam spectroscopy,[9] electronic structure,[7,10] and photochemistry[7,8,11−13] of $[Re(CO)_5]_2$, and the properties and reactivity of the $^{\bullet}Re(CO)_5$ radical,[7,8,13,14] have been extensively studied over the past several decades. The staggered D_{4d} Re−Re dimer has a σ to σ* transition at 305 nm in acetonitrile,[10] and the photolysis at 366 nm in CCl_4 yields $Re(CO)_5Cl$ with high quantum yield (0.4−0.6).[7] A flash photolysis study of $[Re(CO)_5]_2$ in hexane under 1 atm of CO pressure at 22 °C indicated Re−Re dimer formation (eq 1) through bimolecular recombination (eq 2) of $^{\bullet}Re(CO)_5$ radicals with the rate constant 3.7×10^9 M^{-1} s^{-1}.

$$Re{-}Re \rightarrow 2Re \rightarrow Re{-}Re \qquad (1)$$

$$-(1/2)d[Re]/dt = d[Re{-}Re]/dt = k_d[Re]^2 \qquad (2)$$

Molecular beam experiments with $[Re(CO)_5]_2$ in the gas phase showed that the excited state lives only a few

* E-mail: fujita@bnl.gov (E.F.); muckerma@bnl.gov (J.T.M.).

(1) Meyer, T. J.; Casper, J. V. *Chem. Rev.* **1985**, *85*, 187−218.
(2) Scott, S. L.; Espenson, J. H.; Zhu, Z. *J. Am. Chem. Soc.* **1993**, *115*, 1789−1797.
(3) Stufkens, D. J. *Coord. Chem. Rev.* **1990**, *90*, 39−112.
(4) Dahl, L. F.; Ishishi, E.; Rundle, R. E. *J. Chem. Phys.* **1957**, *26*, 1750−1751.
(5) Churchill, M. R.; Amoh, K. N.; Wasserman, H. J. *Inorg. Chem.* **1981**, *20*, 1609−1611.
(6) Flintcroft, N.; Huggins, D. K.; Kaesz, H. D. *Inorg. Chem.* **1964**, *3*, 1123−1130.
(7) Wrighton, M. S.; Ginley, D. S. *J. Am. Chem. Soc.* **1975**, *97*, 2065−2072.
(8) Yang, H.; Snee, P. T.; Kotz, K. T.; Payne, C. K.; Frei, H.; Harris, C. B. *J. Am. Chem. Soc.* **1999**, *121*, 9227−9228.
(9) Freedman, A.; Bersohn, R. *J. Am. Chem. Soc.* **1978**, *100*, 4116−4118.
(10) Levenson, R.; Gray, H. B. *J. Am. Chem. Soc.* **1975**, *97*, 6042−6047.
(11) Wegman, R. W.; Olsen, R. J.; Gard, D. R.; Faulkner, L. R.; Brown, T. L. *J. Am. Chem. Soc.* **1981**, *103*, 6089−6092.

10.1021/ic048910v CCC: $27.50
Published on Web 10/26/2004

picoseconds before dissociation takes place.[9] The fragments formed were $^{\bullet}Re(CO)_5$ radicals, and no loss of CO from the metal was observed in the dissociation process in the gas phase;[9] however, later solution studies indicated the formation of other species as minor intermediates via loss of CO from the $^{\bullet}Re(CO)_5$ radical or $^*[Re(CO)_5]_2$.[1,14] The $^{\bullet}Re(CO)_5$ radical has also been generated in the pulse radiolysis of a variety of organorhenium compounds, including $[Re(CO)_5]_2$ in ethanol, as well as in the flash photolysis of $[Re(CO)_5]_2$ in isooctane.[14] The rate constant for $^{\bullet}Re(CO)_5$ abstracting a Cl atom from CCl_4 in ethanol solution was determined to be $3.9 \times 10^7\ M^{-1}\ s^{-1}$, which is 2 orders of magnitude slower that its dimerization. The dimerization rate constant of $^{\bullet}Re(CO)_5$ in isooctane was $2.7 \times 10^9\ M^{-1}\ s^{-1}$, similar to the value obtained in hexane. More recently, the ultrafast reaction dynamics following 295-nm photodissociation of $[Re(CO)_5]_2$ were studied with 300-fs time resolution in CCl_4 and hexane solutions.[13] A series of DFT calculations on $Re(CO)_5$, $[Re(CO)_5]_2$, and $Re(CO)_9(X)$ ($X = CH_4$, $ClCH_3$) were carried out to identify and characterize the transient species in the time-resolved IR spectra.[13] Experimental results on chlorine atom abstraction by the $Re(CO)_5$ radical and DFT calculations for the final product and transition-state complexes suggested that one-electron oxidative addition of a Cl atom from chlorinated methanes to the $Re(CO)_5$ radical involves neither a 19-electron intermediate nor a charge-transfer intermediate $[(CO)_5Re^+ + {}^-Cl-R]$.[8] The detailed study in CCl_4 indicates that about 23% of the initially excited $[Re(CO)_5]_2$ molecules dissociate to $Re(CO)_5$ species that abstract a Cl atom from the CCl_4 solvent, about 20% of the $^*[Re(CO)_5]_2$ molecules dissociate through a $Re-CO_{eq}$ bond cleavage to form the equatorial solvate, $Re_2(CO)_9(CCl_4)$, and about 55% of the $^*[Re(CO)_5]_2$ molecules revert to their ground state, either via an internal relaxation or through geminate recombination.[13]

Morse and Wrighton introduced a MLCT excited state into the excited-state manifold of a metal−metal bond by replacing CO groups in $[Re(CO)_5]_2$ by phen (phen = 1,10-phenanthroline) to give a mixed dimer $(phen)(CO)_3Re-Re(CO)_5$.[15] They investigated mechanistic aspects of the photochemical reactions and have assigned the lowest energy absorption in $(phen)(CO)_3Re-Re(CO)_5$ to a $d\sigma_{MM} \rightarrow d\pi^*_{phen}$ charge-transfer transition that transfers charge from the metal−metal bonding orbital (d_{z^2} orbital on the Re centers) to an antibonding orbital on the phen ligand. Homolytic bond cleavage of the Re−Re bond then takes place, and the quantum yield of ca. 0.17 is independent of the excitation wavelength from 313 to 633 nm at 25 °C. Morse et al. postulated that the depopulation of the $d\sigma_{MM}$ orbital causes the Re−Re bond to break. Meyer and Caspar, however, argued that the initially formed ^{1}CT state rapidly undergoes internal conversion to the nonbonding $^3d\sigma_{MM}-\pi^*_{phen}$ state, which leads to rapid homolysis of the Re−Re bond. Stufkens later pointed out that the assignment of the lowest-energy absorption of metal−metal bonded complexes may be a mixture of $d\sigma_{MM} \rightarrow \pi^*_{phen}$ and $d\pi_{MM} \rightarrow \pi^*_{phen}$ due to the similar energies of the $d\sigma_{MM}$ and the $d\pi_{MM}$ orbitals.[16,17] Using an analogous explanation to that for the excited photochemistry of chromophore-quencher complexes such as $[Q^+-Re^I(bpy)(CO)_3]^{2+}$ (Q^+ = 4,4′-bipyridinium cation, bpy = 2,2′-bipyridine), where the MLCT state ($[Q^+Re^{II}(bpy^{\bullet-})(CO)_3]^{2+*}$) is followed by fast intramolecular electron transfer to produce the LLCT state ($[(Q^{\bullet})Re^{II}(bpy)(CO)_3]^{2+*}$), Stufkens proposed that the $^3d\pi_{MM}-\pi^*_{phen}$ state of $(phen)(CO)_3Re-Re(CO)_5$ is followed by electron transfer from the Re−Re bond to the Re center with bpy.[16] Thus, the formation of this state gives rise to the homolysis reaction.

While we were investigating CO_2 reduction to CO with $Re(dmb)(CO)_3S$ (dmb = 4,4′-dimethyl-2,2′-bipyridine, S = solvent),[18] a ligand radical produced by either homolysis of $[Re(dmb)(CO)_3]_2$ or one-electron reduction of $Re(dmb)(CO)_3X$, we found that the dimerization is strikingly slow. In THF, the rate constant is $20 \pm 3\ M^{-1}\ s^{-1}$,[19] much slower than that[11,14] of $^{\bullet}Re(CO)_5$ and those[1] of other organometallic radicals, which are typically $10^9\ M^{-1}\ s^{-1}$. The quantum yield of the homolysis of $[Re(dmb)(CO)_3]_2$ is also extremely small (10^{-5}). An 18-electron ligand radical species, $Re(dmb^{\bullet})(CO)_3(THF)$, was proposed as the intermediate on the basis of the spectroscopic data.[18] The dimerization of $Re(dmb^{\bullet})(CO)_3(THF)$ is predicted to proceed through the unfavorable preequilibrium shown in eqs 3 and 4 (NN = dmb), where k_4 is the dimerization rate constant of the $^{\bullet}Re(NN)(CO)_3$ radical.

$$Re(NN^{\bullet})(CO)_3(THF) \rightleftharpoons {}^{\bullet}Re(NN)(CO)_3 + THF \quad (3)$$

$$2\,{}^{\bullet}Re(NN)(CO)_3 \rightarrow [Re(NN)(CO)_3]_2 \quad (4)$$

$$2k_d = 2K_3^2k_4 = 40\ M^{-1}\ s^{-1} \quad (5)$$

Is the fragment of the $[Re(dmb)(CO)_3]_2$ homolysis really an 18-electron ligand radical species instead of an "$18 + \delta$ ($\delta > 0.5$)" or "19-electron"[20] complex? Is $Re(dmb^{\bullet})(CO)_3(THF)$ more stable than a 17-elecron $^{\bullet}Re(dmb)(CO)_3$? Is the further reduced $Re(dmb)(CO)_3^-$ a five-coordinate species? Does a solvent molecule coordinate to $Re(dmb)(CO)_3^-$ to form a six-coordinate species? In order to understand the properties of $Re(dmb)(CO)_3(THF)$ and the photophysics and photochemistry of $[Re(dmb)(CO)_3]_2$, B3LYP hybrid DFT[21−23] and

(12) Gard, D. R.; Brown, T. L. *J. Am. Chem. Soc.* **1982**, *104*, 6340−6347.
(13) Yang, H.; Snee, P. T.; Kotz, K. T.; Payne, C. K.; Harris, C. B. *J. Am. Chem. Soc.* **2001**, *123*, 4204−4210.
(14) Meckstroth, W. K.; Walters, R. T.; Waltz, W. L.; Wojcicki, A.; Dorfman, L. M. *J. Am. Chem. Soc.* **1982**, *104*, 1842−1846.
(15) Morse, D. L.; Wrighton, M. S. *J. Am. Chem. Soc.* **1976**, *98*, 3931−3934.
(16) Stufkens, D. J. *Comments Inorg. Chem.* **1992**, *13*, 359−385.
(17) Stufkens, D. J.; Vlcek, A. *Coord. Chem. Rev.* **1998**, *177*, 127−179.
(18) Hayashi, Y.; Kita, S.; Brunschwig, B. S.; Fujita, E. *J. A. Chem. Soc.* **2003**, *125*, 11976−11987.
(19) In our previous publication,[18] we suppressed the factor of 2 arising from the stoichiometry. We corrected this and recalculated $\Delta H^{\ddagger}$ and $\Delta S^{\ddagger}$. The corrected $\Delta S^{\ddagger}$ is slightly larger than the previously reported value of −14 eu (see Table 1).
(20) Tyler, D. R. *Acc. Chem. Res.* **1991**, *24*, 325−331.
(21) Becke, A. D. *Phys. Rev. A* **1988**, *38*, 3098.
(22) Lee, C.; Yang, W.; Parr, R. G. *Phys. Rev. B* **1988**, *37*, 785.
(23) Miehlich, B.; Savin, A.; Stoll, H.; Preuss, H. *Chem. Phys. Lett.* **1989**, *157*, 200.

fully ab initio RHF and MP2[24−27] calculations on [Re(bpy)(CO)$_3$]$_2$, Re(bpy)(CO)$_3$S, Re(bpy)(CO)$_3$, Re(bpy)(CO)$_3^-$, [Re(CO)$_5$)]$_2$, and Re(CO)$_5$ were performed. We also carried out various experiments on [Re(bpy)(CO)$_3$]$_2$ and Re(bpy)(CO)$_3$S in order to compare them with the dmb analogues. Here, we present theoretical and experimental evidence of the unusually slow dimerization of Re(bpy)(CO)$_3$S.

Experimental Section

Materials. The complexes, Re(dmb)(CO)$_3$OTf,[28,29] Re(dmb)(CO)$_3$Cl,[30,31] Re(bpy)(CO)$_3$OTf, and Re(bpy)(CO)$_3$Cl,[32] were prepared as previously described and characterized by NMR, UV−vis, and IR spectroscopy. Acetonitrile (CH_3CN) and tetrahydrofuran (THF) were purified in the published manner[33] and stored under vacuum over activated molecular sieves (MS) and sodium−potassium alloy (NaK), respectively.

Preparation of Reduced Re(bpy)(CO)$_3$X and Re(dmb)(CO)$_3$X by Na−Hg or Na Mirror. Dark solid [Re(bpy)(CO)$_3$]$_2$ was prepared from a THF solution containing Re(bpy)(CO)$_3$OTf by Na−Hg reduction as previously reported for [Re(dmb)(CO)$_3$]$_2$.[18] The solids were collected, washed with THF, and stored in an argon-filled glovebox. Solutions of the reduced species (0.04−0.10 mM) were prepared under vacuum by either dissolving [Re(bpy)(CO)$_3$]$_2$ or Na mirror reduction of Re(bpy)(CO)$_3$X (X = OTf, Cl) in sealed glassware equipped with an optical cell. Since [Re(bpy)(CO)$_3$]$_2$ and all other reduced species are air- and moisture-sensitive, the solutions for physical measurements were prepared with great care using very dry solvents.

Spectroscopic Measurements. UV−vis spectra were measured on a Hewlett-Packard 8452A diode array spectrophotometer. FTIR spectra were measured on a Mattson Polaris FT-IR spectrometer or a Bruker IFS 66/s spectrometer. NMR spectra were measured on a Bruker UltraShield 400 MHz spectrometer. All CW experiments were performed at 25 °C under vacuum using light from a 150 W xenon lamp with a 380 nm LP filter. The kinetics of the signal-averaged data were analyzed using Levenberg−Marquardt nonlinear least-squares routines written in MATLAB.

DFT and Fully ab Initio RHF and MP2 Calculations. DFT calculations on [Re(bpy)(CO)$_3$]$_2$ and its fragments in the gas phase were carried out using the hybrid B3LYP method[21−23] and a double-ζ basis consisting of the Hay−Wadt (n + 1) VDZ ECP (LANL2DZ) basis[34−36] for Re and the 6-31G basis for H, C, N, and O atoms.[37] The LANL2DZ basis replaces the inner 60 electrons of Re with an effective core potential that includes the one-electron Darwin and mass-velocity relativistic corrections in its definition. Geometry optimizations were performed for the various conformers using the Gaussian 98 package of programs.[24] We carried out additional geometry optimizations with the B3LYP method and the 6-31G* basis[38] for the light atoms using the Gaussian 98 program, and with the RPBE DFT method[39] using the Dmol^3 program[40−42] with the Stuttgart ECP basis for Re[43] and the numerical dnp basis for the light atoms. Single-point energy calculations at the MP2 level of theory at the B3LYP optimized geometries were performed using the Gaussian 98 program,[24] and a few geometry optimizations at the MP2 level of theory[27] were also performed with the Gaussian 03 program.[25] In order to evaluate the solvation effect, we carried out B3LYP/LACVP (LANL2DZ for Re and a numerical version of the 6-31G basis for the light atoms) calculations for several species in THF solution using the Jaguar 5.0 program.[44] Time-dependent B3LYP calculations were carried out with the Gaussian 03 program[25] to predict UV−vis spectra of various species. Additional calculations were performed for the well-characterized [Re(CO)$_5$]$_2$ species and its monomer radical for comparison. The Cartesian coordinates for [Re(bpy)(CO)$_3$]$_2$ conformers and the fragments optimized at the B3LYP-DFT level of theory are presented in Tables S1−S9 (Supporting Information).

Results and Discussion

Experimental Results for [Re(bpy)(CO)$_3$]$_2$. Upon reduction of a yellow solution containing Re(bpy)(CO)$_3$(OTf) in THF (eq 6, NN = bpy), formation of the reddish-purple ligand radical species with characteristic bands at 360, 454, and 486 nm was observed. This species is not stable in THF. Within 1 h, this species converts thermally to a species which has bands at 480, 604, and 808 nm. This change from a reddish-purple solution to a blue-green solution is due to the

(24) Frisch, M. J.; Trucks, G. W.; Schlegel, H. B.; Scuseria, G. E.; Robb, M. A.; Cheeseman, J. R.; Zakrzewski, V. G.; Montgomery, J. A., Jr.; Stratmann, R. E.; Burant, J. C.; Dapprich, S.; Millam, J. M.; Daniels, A. D.; Kudin, K. N.; Strain, M. C.; Farkas, O.; Tomasi, J.; Barone, V.; Cossi, M.; Cammi, R.; Mennucci, B.; Pomelli, C.; Adamo, C.; Clifford, S.; Ochterski, J.; Petersson, G. A.; Ayala, P. Y.; Cui, Q.; Morokuma, K.; Malick, D. K.; Rabuck, A. D.; Raghavachari, K.; Foresman, J. B.; Cioslowski, J.; Ortiz, J. V.; Stefanov, B. B.; Liu, G.; Liashenko, A.; Piskorz, P.; Komaromi, I.; Gomperts, R.; Martin, R. L.; Fox, D. J.; Keith, T.; Al-Laham, M. A.; Peng, C. Y.; Nanayakkara, A.; Gonzalez, C.; Challacombe, M.; Gill, P. M. W.; Johnson, B. G.; Chen, W.; Wong, M. W.; Andres, J. L.; Head-Gordon, M.; Replogle, E. S.; Pople, J. A. *Gaussian 98*, revision A.7; Gaussian, Inc.: Pittsburgh, PA, 1998.

(25) Frisch, M. J.; Trucks, G. W.; Schlegel, H. B.; Scuseria, G. E.; Robb, M. A.; Cheeseman, J. R.; Montgomery, J. A., Jr.; Vreven, T.; Kudin, K. N.; Burant, J. C.; Millam, J. M.; Iyengar, S. S.; Tomasi, J.; Barone, V.; Mennucci, B.; Cossi, M.; Scalmani, G.; Rega, N.; Petersson, G. A.; Nakatsuji, H.; Hada, M.; Ehara, M.; Toyota, K.; Fukuda, R.; Hasegawa, J.; Ishida, M.; Nakajima, T.; Honda, Y.; Kitao, O.; Nakai, H.; Klene, M.; Li, X.; Knox, J. E.; Hratchian, H. P.; Cross, J. B.; Adamo, C.; Jaramillo, J.; Gomperts, R.; Stratmann, R. E.; Yazyev, O.; Austin, A. J.; Cammi, R.; Pomelli, C.; Ochterski, J. W.; Ayala, P. Y.; Morokuma, K.; Voth, G. A.; Salvador, P.; Dannenberg, J. J.; Zakrzewski, V. G.; Dapprich, S.; Daniels, A. D.; Strain, M. C.; Farkas, O.; Malick, D. K.; Rabuck, A. D.; Raghavachari, K.; Foresman, J. B.; Ortiz, J. V.; Cui, Q.; Baboul, A. G.; Clifford, S.; Cioslowski, J.; Stefanov, B. B.; Liu, G.; Liashenko, A.; Piskorz, P.; Komaromi, I.; Martin, R. L.; Fox, D. J.; Keith, T.; Al-Laham, M. A.; Peng, C. Y.; Nanayakkara, A.; Challacombe, M.; Gill, P. M. W.; Johnson, B.; Chen, W.; Wong, M. W.; Gonzalez, C.; Pople, J. A. *Gaussian 03*, revision B.04; Gaussian, Inc.: Pittsburgh, PA, 2003.

(26) Roothan, C. C. J. *Rev. Mod. Phys.* **1951**, *23*, 69.

(27) Møller, C.; Plesset, M. S. *Phys. Rev.* **1934**, *46*, 618.

(28) Koike, K.; Hori, H.; Ishizuka, M.; Westwell, J. R.; Takeuchi, K.; Ibusuki, T.; Enjouji, K.; Konno, H.; Sakamoto, K.; Ishitani, O. *Organometallics* **1997**, *16*, 5724−5729.

(29) Gibson, D. H.; Yin, X. *J. Am. Chem. Soc.* **1998**, *120*, 11200−11201.

(30) Breikss, A. I.; Abruña, H. D. *J. Electroanal. Chem.* **1986**, *201*, 347−358.

(31) Wrighton, M.; Morse, D. L. *J. Am. Chem. Soc.* **1974**, *96*, 998−1003.

(32) Casper, J. P.; Meyer, T. J. *J. Am. Chem. Soc.* **1983**, *87*, 952−957.

(33) Riddick, J. A.; Bunger, W. B.; Sakano, T. K. *Organic Solvents, Physical Properties and Methods of Purification*, 4th ed.; Wiley: New York, 1986.

(34) Hay, P. J.; Wadt, W. R. *J. Chem. Phys.* **1985**, *82*, 299−310.

(35) Hay, P. J.; Wadt, W. R. *J. Chem. Phys.* **1985**, *82*, 270−283.

(36) Wadt, W. R.; Hay, P. J. *J. Chem. Phys.* **1985**, *82*, 284−298.

(37) Hehre, W. J.; Ditchfield, R.; Pople, J. A. *J. Chem. Phys.* **1972**, *56*, 2257.

(38) Hariharan, P. C.; Pople, J. A. *Mol. Phys.* **1974**, *27*, 209.

(39) Hammer, B.; Hansen, L. B.; Norskov, J. K. *Phys. Rev. B* **1999**, *59*, 7413.

(40) Delley, B. *J. Chem. Phys.* **1990**, *92*, 508.

(41) Delley, B. *J. Chem. Phys.* **2000**, *113*, 7756.

(42) MS Modeling, Release 2.2, San Diego: Accelrys Inc., 2002.

(43) Dolg, M.; Wadig, U.; Stoll, H.; Preuss, H. *J. Chem. Phys.* **1987**, *86*, 866.

(44) *Jaguar 5.0*; Schrödinger, L.L.C.: Portland, OR 1991−2003.

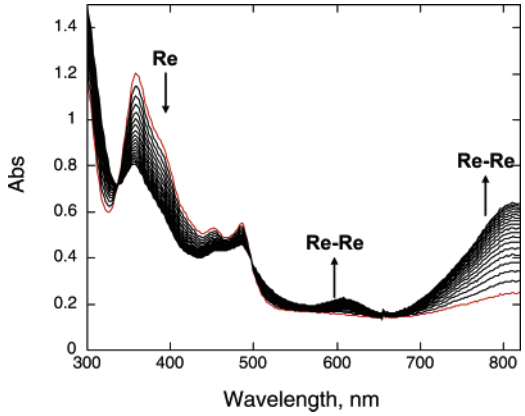

Figure 1. Dimerization of Re(bpy)(CO)$_3$(THF). Spectral change of a THF solution containing 3.6 × 10^{-5} M [Re(bpy)(CO)$_3$]$_2$ monitored every 70 s after photolysis (>380 nm). The spectrum shown in red is mainly that of Re(bpy)(CO)$_3$(THF).

dimerization of Re(bpy)(CO)$_3$(THF) (eq 7) as previously studied in the case of Re(dmb)(CO)$_3$(THF).[18] Almost all these absorption bands are blue shifted compared to those of dmb analogues: Re(dmb)(CO)$_3$(THF), 356, 467, and 496 nm; [Re(dmb)(CO)$_3$]$_2$, 480, 620 and 818 nm. Since the solubility of [Re(bpy)(CO)$_3$]$_2$ in THF is low, dark greenish solid [Re(bpy)(CO)$_3$]$_2$ can be precipitated from a THF solution containing the one-electron reduced species of Re(bpy)(CO)$_3$(OTf). The IR spectrum of [Re(bpy)(CO)$_3$]$_2$ in THF shows ν_{CO} at 1990, 1952, 1886, and 1863 cm^{-1} and is similar to that previously reported (1988, 1951, 1887, and 1859 cm^{-1}) by Stor et al.[45] While their UV−vis spectrum of [Re(bpy)(CO)$_3$]$_2$ is similar to ours, their spectrum assigned as that of Re(bpy)(CO)$_3$(THF)$^+$ seems to be a mixture of [Re(bpy)(CO)$_3$]$_2$ and Re(bpy)(CO)$_3$(THF).

$$\mathrm{Re(NN)(CO)_3S^+ + e^- \rightarrow Re(NN)(CO)_3S} \qquad (6)$$

$$\mathrm{2Re(NN)(CO)_3S \rightarrow [Re(NN)(CO)_3]_2 + 2S} \qquad (7)$$

$$\mathrm{[Re(NN)(CO)_3]_2 + 2S + h\nu \rightarrow 2Re(NN)(CO)_3S} \qquad (8)$$

Upon photolysis (λ > 380 nm) of a THF solution containing 0.025−0.1 mM [Re(bpy)(CO)$_3$]$_2$, Re−Re bond homolysis takes place to form the monomer, with characteristic absorptions at 454 and 486 nm (eq 8) for the bpy anion radical as previously found for [Re(dmb)(CO)$_3$]$_2$.[18] As shown in Figure 1, the monomer reversibly re-forms the dimer after photolysis at 25 °C. Formation of the dimer is surprisingly slow and is second order in [Re(bpy)(CO)$_3$(THF)] with k_d = 11 ± 4 M^{-1} s^{-1} (eqs 2 and 7) at 25 °C in THF as seen in Figure 2. While the decay of Re(bpy)(CO)$_3$(THF) and growth of [Re(bpy)(CO)$_3$]$_2$ are fit well with second-order kinetics, and the recovery of [Re(bpy)(CO)$_3$]$_2$ is >95%, the observed rates are slightly scattered because of the slow dimerization of extremely reactive Re(bpy)(CO)$_3$(THF). We carefully prepared a number of THF solutions containing [Re(bpy)(CO)$_3$]$_2$ by vacuum distillation of THF stored over NaK and flame-sealed the glassware before the kinetic measurements; however, impurities in the system seem to cause the deviations of the observed rates. The dimerization process for [Re(dmb)(CO)$_3$]$_2$ has been previously observed in THF.[18] It was slightly faster (k_d = 20 ± 3 M^{-1} s^{-1}). These dimerization constants for [Re(NN)(CO)$_3$]$_2$ are strikingly small compared to that of typical organometallic radicals including •Re(CO)$_5$ (2.7 × 10^9 M^{-1} s^{-1} in isooctane).[14]

(45) Stor, G. J.; Hartl, F.; Outersterp, J. W. M. V.; Stufkens, D. J. *Organometallics* **1995**, *14*, 1115−1131.

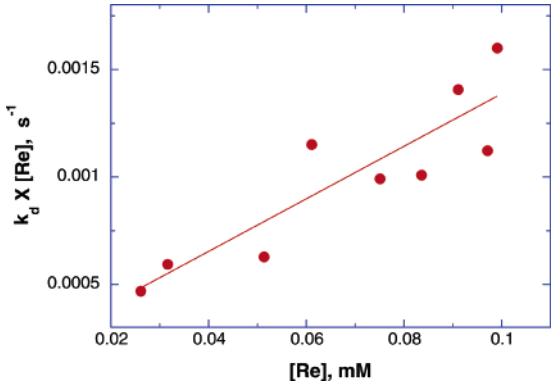

Figure 2. Plot of observed rate constants for dimerization of Re(bpy)(CO)$_3$(THF) at 25 °C vs Re(bpy)(CO)$_3$(THF) concentration.

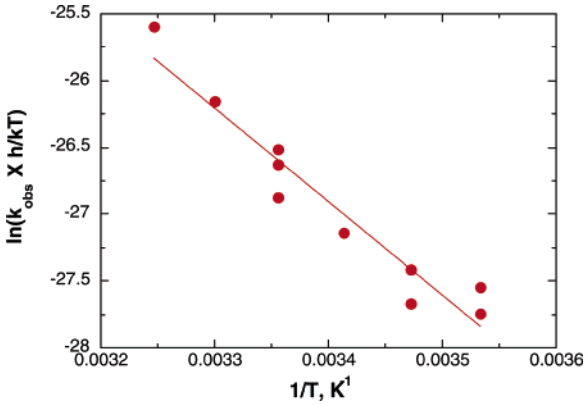

Figure 3. Plot of ln(k_{obs} × h/kT) vs 1/T for the dimerization of Re(bpy)(CO)$_3$(THF).

$$k_{obs} = \frac{k_B T}{h} e^{-\Delta H^{\ddagger}/RT} e^{\Delta S^{\ddagger}/R} \qquad (9)$$

Activation parameters (eq 9) for the dimerization reaction (eq 7) of Re(bpy)(CO)$_3$(THF) in THF are obtained from the Eyring plot (Figure 3) of ln(k_{obs} × h/$k_B T$) versus 1/T for the dimerization reaction of Re(bpy)(CO)$_3$(THF). The rate constants for the dimerization (k_{obs}'s) were measured at 10, 15, 20, 25, 30, and 35 °C. The activation enthalpy ($\Delta H^{\ddagger}$ = 14 kcal mol^{-1}) and entropy ($\Delta S^{\ddagger}$ = −6 cal mol^{-1} K^{-1}) are calculated from the slope and the intercept, respectively (Figure 3). The spectral, thermodynamic, and kinetic properties are summarized in Table 1. Since bpy is a less basic ligand than dmb, the solvent can coordinate more strongly to the metal. This is consistent with the higher activation barrier (14 kcal mol^{-1}) of the dimerization of Re(bpy)(CO)$_3$(THF) than that (11 kcal mol^{-1}) of Re(dmb)(CO)$_3$(THF) and the assumption that the dimerization process involves eqs 3 and 4.

Table 1. Comparison of Properties of $Re(NN)(CO)_3$-Type Complexes in THF

property		bpy	dmb[a]
UV−vis λ_{max}, nm (ϵ, $mM^{-1}\,cm^{-1}$)	$Re(NN)(CO)_3Cl$	388 (3.2), 294 (16.7), 240 (19.0)	384 (3.4), 294 (17.2), 240 (19.7)
	$[Re(NN)(CO)_3]_2$	808 (21.2), 604 (7.2), 480 (9.2)	818 (17.6), 620 (5.8), 520sh (7.2), 480 (8.1)
	$Re(NN)(CO)_3(THF)$	486, 454, 360	496, 467, 356
	$Re(NN)(CO)_3^-$	570 (13.8), 280 (25.7)	582 (13.1), 378sh (8.8), 282 (24.5)
IR ν_{CO}, cm^{-1}	$Re(NN)(CO)_3Cl$	2019, 1917, 1895	
		2023,[b] 1914,[b] 1902[b]	2021,[b] 1914(br)[b]
	$[Re(NN)(CO)_3Cl]^-$	1998,[b] 1880,[b] 1866[b]	
	$Re(NN)(CO)_3S$	2017,[b] 1902(br)[b]	2012,[b] 1904(br)[b] 2008, 1897(br)
	$[Re(NN)(CO)_3]_2$	1990, 1952, 1886, 1863	1976, 1947, 1877, 1855
	$Re(NN)(CO)_3^-$	1947, 1843(br)	1940, 1832(br)
k_d, $M^{-1}\,s^{-1}$		11	20
$\Delta H^{\ddagger}$, kcal mol^{-1}		14	11
$\Delta S^{\ddagger}$, eu		−6	−17

[a] In ref 18. [b] In CH_3CN.

Table 2. Geometric Parameters of the Skewed *cis*-$[Re(bpy)(CO)_3]_2$ and Skewed *trans*-$[Re(bpy)(CO)_3]_2$ Conformers

property/species	skewed *cis* B3LYP gas phase	skewed *cis* B3LYP THF solution	skewed *cis* MP2 gas phase	skewed *trans* B3LYP gas phase	skewed *trans* B3LYP THF solution	skewed *trans* MP2 gas phase
			Bond Distances (Å)			
Re−Re	3.254	3.229	3.014	3.229	3.209	3.024
Re−N	2.144, 2.140	2.162, 2.161	2.125, 2.114	2.158, 2.156	2.171, 2.171	2.128, 2.118
Re−C (equatorial CO)	1.931, 1.921	1.921, 1.920	1.948, 1.932	1.923, 1.917	1.920, 1.919	1.939, 1.926
Re−C (axial CO)	1.903	1.894	1.927	1.908	1.894	1.932
			Bond Angles (deg)			
Re−Re−C (axial CO)	168.4	168.0	170.4	167.0	166.2	171.6
Re−C−O (axial CO)	178.3	176.6	179.0	177.2	174.8	177.9
Re−Re−N	94.8, 90.3	97.0, 89.9	92.0, 88.4	93.7, 93.3	97.2, 96.4	90.0, 89.5
Re−Re−C (equatorial CO)	85.2, 77.4	87.1, 74.7	86.2, 81.6	81.0, 79.0	80.2, 75.4	85.0, 83.4
N−Re−N	75.5	75.1	75.5	75.0	74.8	75.5
C−Re−C (equatorial COs)	91.2	90.4	89.5	90.2	89.7	88.9
			Dihedral Angles (deg)			
N−Re−Re−N	54.5	56.1	52.2	139.1	140.5	134.8
C−Re−Re−C (equatorial COs)	54.0	55.1	51.4	140.4	140.8	136.4
C−Re−Re−C (axial COs)	106.8	143.2	94.1	151.1	159.3	124.0
Re−Re−C−O (axial CO)	17.0	−8.7	27.9	10.4	−0.9	20.6

Theoretical Studies of the Geometry of $[Re(bpy)(CO)_3]_2$. Since single crystals are not available for determining the geometric structure of $[Re(dmb)(CO)_3]_2$ or $[Re(bpy)(CO)_3]_2$, we turned to theory. Initial DFT calculations on $[Re(bpy)(CO)_3]_2$ in the gas phase were carried out using the hybrid B3LYP method. Geometry optimizations were performed for both the *trans* and *cis* conformers. The *trans*-$[Re(bpy)(CO)_3]_2$ optimization was constrained to C_{2h} symmetry, while that for *cis*-$[Re(bpy)(CO)_3]_2$ was constrained to C_{2v} symmetry. Stationary points were found for both the *trans* and *cis* conformers, but a subsequent vibrational frequency analysis indicated that both these conformers had a single imaginary frequency corresponding to rotation about the Re−Re bond. Thus, both the *trans* and *cis* conformers are transition states separating one or more "skewed" intermediate conformations. Subsequent geometry optimizations and vibrational frequency analyses revealed two local minima of C_2 symmetry: skewed *trans* (rotated 41° about the Re−Re bond from the *trans* configuration) and skewed *cis* (rotated 55° about the Re−Re bond from the *cis* configuration) conformers. Table 2 lists the principal geometric properties of the optimized skewed *cis*-$[Re(bpy)(CO)_3]_2$ and skewed *trans*-$[Re(bpy)(CO)_3]_2$ species in the gas phase and in THF solution, and Figure 4 shows the two gas-phase optimized structures. The Re−Re bond is rather long in all the structures, even longer than our calculated 3.154 Å for $[Re(CO)_5]_2$ (see later section). The B3LYP/6-31G Re−Re bond distances in the gas phase are 3.229 and 3.254 Å for skewed *trans* and skewed *cis* conformers, respectively. Averaged Re−N distances are 2.157 and 2.142 Å for skewed *trans* and skewed *cis* conformers, respectively. When the skewed *cis* conformer is in THF solution, the Re−Re bond becomes shorter (3.229 Å) while the Re−N distance becomes longer (2.162 Å). While the Re−C (CO_{eq}) distance does not change, the Re−C (CO_{ax}) becomes ∼0.01 Å shorter. A similar trend is observed for the skewed *trans* conformer. In addition to the rotation about the Re−Re bond, these dimers are slipped from a collinear OC−Re−Re−CO configuration ($\angle Re-Re-CO_{ax} \approx 168°$). Both the skewed *trans* and skewed *cis* conformers have a zigzag geometry for $OC_{ax}-Re-Re-CO_{ax}$. The two bpy moieties are not strictly perpendicular to the Re−Re axis in either conformer, but in the skewed *trans* conformer they are more parallel to each other than in the skewed *cis* conformer.

The skewed *trans* conformer was computed to have the lower energy for the basis set and level of theory employed.

Table 3. Calculated Energies (kcal/mol) of [Re(bpy)(CO)$_3$]$_2$ Conformers Relative to Skewed *trans*-[Re(bpy)(CO)$_3$]$_2$ with Various Levels of Theory Using Gaussian

species	B3LYP HW ECP/6-31G	B3LYP HW ECP/6-31G*	MP2//B3LYP HW ECP/6-31G	MP2 HW ECP/6-31G
cis-[Re(bpy)(CO)$_3$]$_2$ ^{1}A$_1$ (C_{2v})	13.41	11.00	12.25	
trans-[Re(bpy)(CO)$_3$]$_2$ ^{1}A$_g$ (C_{2h})	3.01	3.26	6.49	
skewed *cis*-[Re(bpy)(CO)$_3$]$_2$ ^{1}A (C_2)	5.84	4.72	2.96	0.58

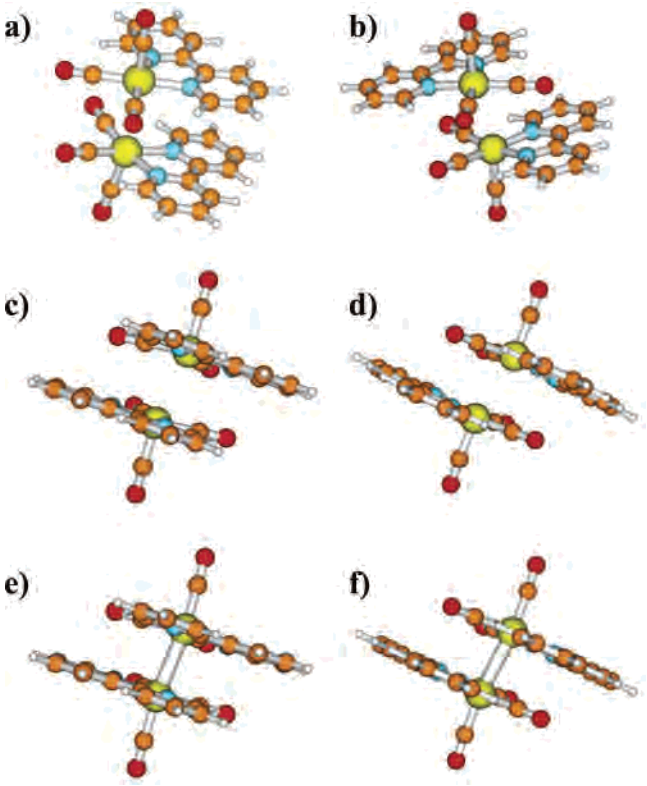

Figure 4. Structures of the skewed *cis*-[Re(bpy)(CO)$_3$]$_2$ conformer in the left column (a, c, and e) and structures of the skewed *trans* conformer in the right column (b, d, and f). Structures a and c are different views of the optimized B3LYP geometry, as are structures b and d. Structures e and f are the optimized MP2 geometries viewed as in c and d, respectively. The shorter Re−Re bond length and flatter bpy rings are apparent in the MP2 optimized structures.

Unless otherwise specified, here and throughout this work we use the term "energy" to mean total electronic energy without zero-point energy corrections. The difference in gas-phase energy between these two conformers was 5.8 kcal/mol as can be seen in Tables 3 and 4. This value is reduced to 5.5 kcal/mol upon inclusion of the zero-point energy. We computed the thermodynamic properties of the gas-phase dimerization reaction from the electronic energies and vibrational frequencies of the two conformers of the dimer as well as those of the monomer (see below). At 298 K, we calculated the gas-phase dimerization reaction forming the skewed *trans* conformer to have a $\Delta H°$ of −29.1 kcal/mol and a $\Delta G°$ of −12.7 kcal/mol. The $\Delta H°$ for the formation of the skewed *cis* conformer was calculated to be −23.5 with a $\Delta G°$ of −8.0 kcal/mol. The smaller negative $\Delta G°$ values relative to the $\Delta H°$ values are the result of the large negative $\Delta S°$ associated with dimerization. At this level of theory, the difference in gas-phase dimerization enthalpy and free energy values is computed to be −5.6 and −4.7 kcal/mol, respectively, favoring the skewed *trans* conformer.

Table 4. Energetics of Various Processes (in kcal/mol) Involving [Re(bpy)(CO)$_3$]$_2$ Conformers, Fragments, and Related Species from B3LYP DFT Calculations

property	Gaussian B3LYP HW ECP/6-31G	Jaguar B3LYP LACVP
THF Binding Energy		
gas phase	18.2	17.8
$\Delta H°$ in gas phase	16.3	
$\Delta H°$ in THF solution		7.2
Dimer Binding Energy: Skewed *trans* Conformer		
gas phase	31.0	31.5
THF solution		25.3
$\Delta H°$ in gas phase		29.1
$\Delta H°$ in THF solution		22.8
Dimer Binding Energy: Skewed *cis* Conformer		
gas phase	25.2	25.6
THF solution		22.4
$\Delta H°$ in gas phase		23.5
$\Delta H°$ in THF solution		20.3
Energy Difference between Skewed *cis* and Skewed *trans* Conformers		
gas phase	5.8	5.9
$\Delta H°$ in the gas phase	5.6	
THF solution		2.9
$\Delta H°$ in THF solution		1.7
gas-phase energy difference between *trans* and skewed *trans* conformers	3.0	
gas-phase energy difference between *cis* and skewed *trans* conformers	13.4	
gas-phase [Re(CO)$_5$]$_2$ dimer binding energy	42.3	
Re−Cl Bond Energy in Re(bpy)(CO)$_3$Cl		
gas phase		80.9
THF solution		90.2
Re(bpy)(CO)$_3$Cl$^-$ → Re(bpy)(CO)$_3$ + Cl$^-$ Reaction Energy		
gas phase		+16.0
THF solution		−21.8

We attempted to confirm this finding by carrying out geometry optimizations with the B3LYP method and the 6-31G* basis for the light atoms, and with the RPBE DFT method with the Stuttgart ECP basis[43] for Re and the numerical dnp basis for the light atoms. We also carried out single-point energy calculations with the LANL2DZ/6-31G basis at the MP2 level of theory at the B3LYP optimized geometries. In the MP2//B3LYP calculations, the energy difference between the two conformers was reduced to the difference between their solvation energies (see later). Since the assignment of the geometry of the lowest-energy conformer is important for the interpretation of the experimental data, we carried out a full geometry optimation of both the skewed *trans* and skewed *cis* conformers at the MP2/6-31G level of theory using 85 occupied orbitals and all 261 virtual orbitals in the treatment of electron correlation. Tables 3 and S9 summarize the results of these calculations. All the DFT methods placed the skewed *cis* conformer 3−6

kcal/mol above the skewed *trans* conformer, always slightly above the *trans* transition state. The MP2//B3LYP calculations placed the *cis* conformer 3 kcal/mol above the skewed *trans* one, but 3.5 kcal/mol below the *trans* transition state. The optimized gas-phase MP2 energy of the skewed *cis* conformer is only 0.6 kcal/mol higher than that of the skewed *trans* conformer (see Table 3). Given the fact that the solvation energy of the skewed *cis* conformer is about 3.0 kcal/mol greater than that of the skewed *trans* conformer (see later), there can be no doubt that the skewed *cis* conformer is energetically favored in THF solution. The MP2/6-31G optimization of the skewed *cis* and the skewed *trans* conformers, starting from their B3LYP/6-31G optimized geometries, resulted in a decrease in energy of 12.4 and 10.0 kcal/mol, respectively, and was accompanied by significant changes in structure. Most notable among these were a decrease in the Re−Re bonds to 3.00 and 3.02 Å from 3.25 and 3.23 Å, respectively, and a flattening of the bpy moieties as they became oriented more nearly perpendicular to the Re−Re axis (see Figure 4 and Table 2). The zigzag geometries of $OC_{ax}-Re-Re-CO_{ax}$ predicted by the B3LYP/6-31G calculations for both conformers become more linear, and the skewing angles become 52° and 45° for the skewed *cis* and skewed *trans* conformers, respectively. We believe the MP2 geometric properties in Table 2 to be the more reliable gas-phase values.

Because the experiments were carried out in THF solution, and the computed dipole moments of the skewed *trans* (7.12 D) and skewed *cis* (17.85 D) conformers were quite different, we carried out B3LYP/LACVP calculations for these two conformers in THF solution using the Jaguar 5.0 program.[44] Owing to slight differences in implementation, the gas-phase energies in the Jaguar results were 2.35 and 2.29 kcal/mol lower for the skewed *trans* and skewed *cis* conformers, respectively, than those obtained with Gaussian 98 (Table S10). The difference in gas-phase energy between these two conformers (5.9 kcal/mol) was reduced to 2.9 kcal/mol in THF solution because the solvation energy of the skewed *cis* conformer was 3.0 kcal/mol larger than that for the skewed *trans* conformer (22.6 vs 19.6 kcal/mol, respectively). This difference in solvation energy more than offsets the small (0.6 kcal/mol) gas-phase MP2/6-31G energy difference between the two conformers.

Although the crystallographic structure of the isoelectronic manganese complex, $[Mn(bpy)(CO)_3]_2$, has not been solved, the structure of the 2,2′-biphosphine analogue $[Mn(tmbp)(CO)_3]_2$ (tmbp = 4,4′,5,5′-tetramethyl-2,2′-biphosphine) has been reported.[46] This dimer was obtained by chemical reduction of $Mn(tmbp)(CO)_3Br$ by sodium naphthalenide in dimethoxyethane. The coordination geometry of both Mn centers is nearly octahedral, and the two tmbp ligands are twisted about the Mn−Mn bond by 40° from the *cis* position. The Mn−Mn bond distance is 3.060 Å, which is rather long compared to that of $[Mn(CO)_5]_2$ (2.9038 Å).[5] The structure of the Mn dimer is similar to the calculated structure of the skewed *cis*-$[Re(bpy)(CO)_3]_2$ species except the two bpy ligands are 12° more twisted about the Re−Re bond.

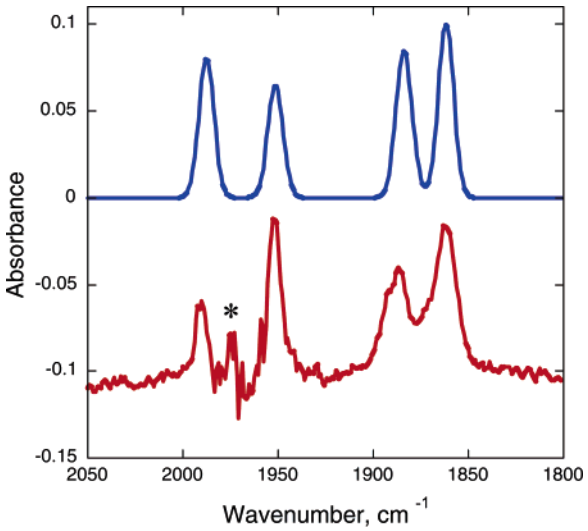

Figure 5. Calculated and observed ν_{CO} for $[Re(bpy)(CO)_3]_2$ in THF. The calculated spectrum is plotted with line broadening (Gaussian with $\sigma = 4$ cm^{-1}) and shifted +57 cm^{-1} to match the observed spectrum. ∗ Due to THF absorption correction.

The computed IR spectra of the $[Re(bpy)(CO)_3]_2$ conformers in THF solution were compared to the experimental spectrum in the CO stretch region. The experimental spectrum exhibits four distinct CO stretching peaks at 1990, 1952, 1886, and 1863 cm^{-1}. Only the skewed *cis* conformer has a computed spectrum that agrees well with experiment; the computed spectrum shifted 57 cm^{-1} to higher frequency matches all features of the experimental one extremely well as shown in Figure 5. The solution-phase CO stretching frequencies (1931, 1894, 1827, and 1805 cm^{-1}) computed with Jaguar 5.0 are actually shifted significantly to the red from the corresponding gas-phase frequencies (1970, 1941, 1886, and 1867 cm^{-1}) computed with Gaussian 98, which are closer to the observed frequencies, but the pattern of spacing and intensity for the solution-phase spectrum for skewed *cis*-$[Re(bpy)(CO)_3]_2$ best matches the experimental spectrum. The predicted gas-phase Re−Re bond energies of the skewed *trans* and skewed *cis* conformers are 31.0 and 25.2 kcal/mol (31.5 and 25.6 with Jaguar), respectively, and the solution-phase Re−Re bond energies are computed (with Jaguar) to be 25.3 and 22.4 kcal/mol.

Because of the distorted geometry of the skewed *cis*-$[Re(bpy)(CO)_3]_2$ species, it is somewhat difficult to characterize the metal−metal bonding character of the molecular orbitals (Figure 6). Nevertheless, it is clear that the HOMO is a $d\sigma_{MM}$ orbital, the LUMO is a bpy π^* orbital, the LUMO + 1 is a peculiar mixture of $d\sigma_{MM}$, bpy π^*, and axial CO* character, and the LUMO + 2 is a bpy π^* orbital (Figure 6). Both the HOMO and LUMO + 1 orbitals have substantial p character in addition to the expected d character on the metal centers. In the HOMO, this involves p_x and p_z, while in the LUMO + 1 it involves p_y. There is also considerably more bpy* and axial CO* character in the LUMO + 1 than in the HOMO. While the skewed *cis* conformer has a classic unoccupied σ_{MM}* orbital at LUMO + 28 (see Figure S1),

(46) Hartl, F.; Mahabiersing, T.; Le Floch, P.; Mathey, F.; Ricard, L.; Rosa, P.; Zalis, S. *Inorg. Chem.* **2003**, *42*, 4442−4455.

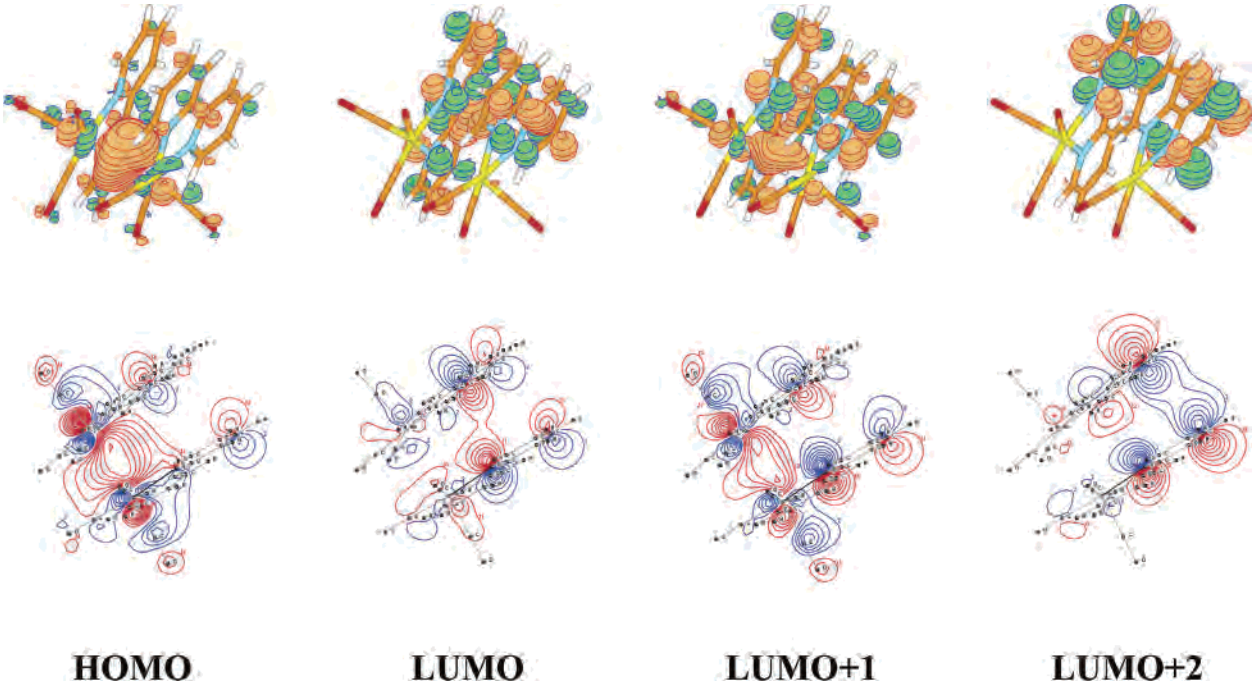

Figure 6. B3LYP/6-31G frontier orbitals: HOMO, LUMO, LUMO + 1, and LUMO + 2 for the skewed *cis*-[Re(bpy)(CO)$_3$]$_2$.

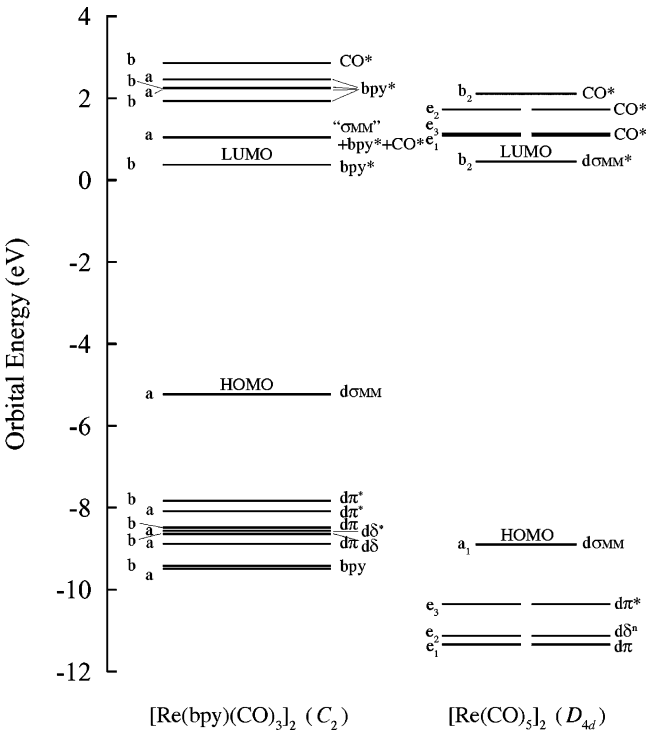

Figure 7. Energy diagram (from HF calculations) for the skewed *cis*-[Re(bpy)(CO)$_3$]$_2$ and staggered [Re(CO)$_5$]$_2$ species.

and LUMO + 17 and LUMO + 27 also have significant "σ_{MM}*" character, there are no low-lying unoccupied orbitals that are primarily σ antibonding between the two metal centers. In these B3LYP calculations, however, the LUMO + 8 orbital is weakly σ antibonding (see Figure S2), and the lowest-energy absorption is predicted to be a d$\sigma_{MM} \rightarrow$ bpy π* charge-transfer transition as shown in Figure 7. Interestingly, the skewed *trans* conformer also has σ_{MM}* as LUMO + 28 (Figure S3). These results are consistent with the dimer having a low quantum yield for photodissociation, and support the notion that the photodissociation mechanism is not a direct one-electron process.

Time-dependent B3LYP calculations of skewed *cis*-[Re(bpy)(CO)$_3$]$_2$ were carried out to understand the electronic transition energies and oscillator strengths. The HOMO to LUMO transition (with a small contribution from the HOMO to LUMO + 2 transition) is predicted to occur at 771 nm with an oscillator strength of 0.1381. The HOMO to LUMO + 1 transition (with a small contribution from the HOMO − 1 to LUMO and the HOMO to LUMO + 5 transitions) is predicted to occur at 605 nm with an oscillator strength of 0.0500. These are followed by the HOMO to LUMO + 2 transition at 543 nm with an oscillator strength of 0.0517, the HOMO − 1 to LUMO transition (with some contribution from the HOMO to LUMO + 3 and HOMO to LUMO + 5 transitions) at 495 nm with an oscillator strength of 0.007, and the HOMO to LUMO + 3 transition (with some contribution from the HOMO − 1 to LUMO transition) at 486 nm with an oscillator strength of 0.0291. These transition energies and intensities are in excellent agreement with the experimental UV−vis spectrum (Figure 8, top). Since the HOMO and HOMO − 1 are dσ_{MM} and dπ_{MM}* orbitals, respectively, and the LUMO and LUMO + n (n = 1−5) are bpy π*-based orbitals, these transitions are clearly MLCT transitions (although the HOMO to LUMO + 1 transition is at least in part dσ_{MM} to dσ_{MM}). The theoretical results are consistent with the experimental conclusion of the MLCT assignment from the fact that polar solvents cause a shift of these visible transitions to higher energy.

Although Stufkens postulated that the lowest energy absorption of metal−metal bonded complexes such as (phen)(CO)$_3$Re−Re(CO)$_5$ may be a mixture of d$\sigma_{MM} \rightarrow \pi_{phen}$* and d$\pi_{MM} \rightarrow \pi_{phen}$*,[16] only the d$\sigma_{MM} \rightarrow \pi_{bpy}$* transition

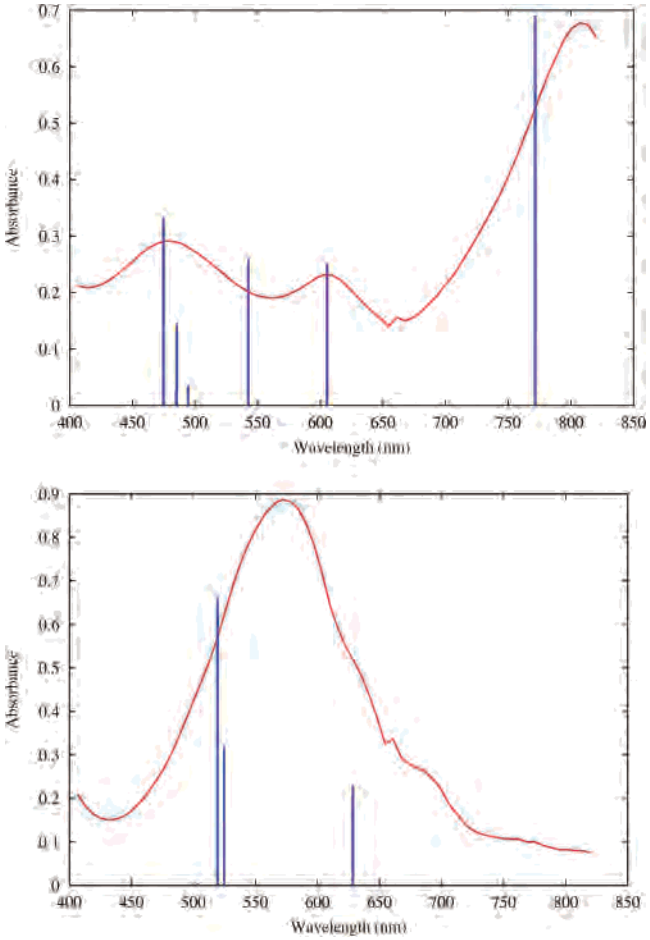

Figure 8. Observed UV−vis spectrum in THF and calculated absorption bands with oscillator strength multiplied by 5 for skewed *cis*-[Re(bpy)(CO)$_3$]$_2$ (top) and Re(bpy)(CO)$_3^-$ (bottom).

is predicted to contribute to the lowest energy absorption (771 nm), and the dπ_{MM}* → π_{bpy}* transition is mixed into the absorptions at 605, 495, and 486 nm in [Re(bpy)(CO)$_3$]$_2$. Therefore, visible light absorption may lead to rapid internal conversion to yield the ^{3}dπ_{MM}−π_{bpy}*, followed by an electron transfer from σ_{MM} to dπ_{MM}* to form the $^3\sigma_{MM}$−π_{bpy}* state in a mannor analogous to that proposed by Stufkens.[16] However, the quantum yield of the homolysis reaction is extremely low, and there is no evidence for this mechanism of the bond homolysis for [Re(NN)(CO)$_3$]$_2$. Although our time-dependent DFT calculation did not clearly indicate the involvement of the HOMO to LUMO + 8 transition in visible absorption (>486 nm), it is quite possible that such a transition may occur at shorter wavelength. We propose that the population of the weakly σ antibonding LUMO + 8 orbital may cause the Re−Re bond to weaken and find some pathway to break. However, it should be noted that the LUMO + 8 exhibits π bonding to the equatorial CO ligands as well as metal−metal "σ" antibonding character; therefore, the direct Re−Re bond cleavage cannot be expected. In fact, in our previous flash photolysis experiments on [Re(dmb)(CO)$_3$]$_2$ in THF, we did not observe formation of (the long-lived) Re(dmb)(CO)$_3$(THF) monomer species, consistent with the low quantum yield.[18] We are currently carrying out DFT and ab initio RHF/MP2 calculations on (bpy)(CO)$_3$Re−Re(CO)$_5$ as a model of (phen)(CO)$_3$Re−Re(CO)$_5$ and will publish the results in a forthcoming paper.

Theoretical Study of [Re(CO)$_5$]$_2$. DFT calculations on [Re(CO)$_5$]$_2$ and its constituent monomer, Re(CO)$_5$, in the gas phase were carried out using the hybrid B3LYP method.[47] Geometry optimizations were performed for the D_{4d} staggered conformer, as indicated by the X-ray structure.[4,5] The calculated B3LYP (Gaussian 98)[24] gas-phase Re−Re bond length is 3.154 Å, longer than those found in crystal structures: 3.02[4] and 3.041[5] Å. The calculated Re−Re bond is also slightly longer than the 3.12 Å value[13] previously obtained using a similar basis and the Jaguar program.[44] However, the calculated MP2 Re−Re bond is 2.959 Å with Re−C$_{eq}$ and Re−C$_{ax}$ bonds of 1.944 and 1.999 Å, respectively, similar to those (1.929 and 1.987 Å) found in the X-ray structure.[5] The Re−Re bond energy was calculated using the hybrid B3LYP method to be 42.3 kcal mol^{-1} and is smaller than the gas-phase experimental enthalpy value of 51.1 kcal mol^{-1} based on the electron-impact ionization potentials using mass spectroscopy.[48]

Hartree−Fock calculations were also carried out for both [Re(CO)$_5$]$_2$ and skewed *cis*-[Re(bpy)(CO)$_3$]$_2$ in order to construct molecular orbital energy diagrams. Figure 7 compares the orbital energies and assignments of [Re(CO)$_5$]$_2$ and skewed *cis*-[Re(bpy)(CO)$_3$]$_2$ at the Hartree−Fock level of theory (at which orbital energies represent one-electron ionization potentials[49]). The HOMO and LUMO of [Re(CO)$_5$]$_2$ are dσ_{MM} and dσ_{MM}*, respectively. The degenerate HOMO − 1, HOMO − 2, and HOMO − 3 are dπ_{MM}*, dδ_{MM}^n, and dπ_{MM}, respectively. Here we use the superscript "n" to denote nonbonding δ orbitals arising from zero overlap due to the staggered geometry. The LUMO + 1 and LUMO + 2 are both CO* orbitals.

For [Re(CO)$_5$]$_2$, time-dependent DFT calculations indicate that the lowest lying (degenerate) electronic state (HOMO to LUMO + 1) is predicted to lie 359 nm above the ground state, but has no oscillator strength. Next comes another degenerate state (HOMO to LUMO + 2) at 351 nm that has an oscillator strength of only 0.0002. Then come the strong HOMO to LUMO transition at 315 nm with an oscillator strength of 0.3374, the (degenerate) HOMO − 1 to LUMO transition at 304 nm with an oscillator strength of 0.0180, the (degenerate) HOMO − 1 to (degenerate) LUMO + 2 (CO*) transition at 283 nm with an oscillator strength of 0.0896, and HOMO to LUMO + 4 (CO*) and LUMO + 5 (CO*) transitions at 271 nm with an oscillator strength of 0.0002. The transitions at 315 and 304 nm are probably blended, with a distinct transition at 283 nm. Extended-Hückel-type molecular calculations were previously carried out to assign the several absorption bands of [Re(CO)$_5$]$_2$ at 70 K.[10] The dσ_{MM} to dσ_{MM}*, dσ_{MM} to CO*, and dπ_{MM} to CO* transitions were assigned for absorptions at 306, 278, and 262 nm, respectively. Our computed UV−vis spectrum is in excellent agreement with the previous experimental spectrum at 300 K (λ_{max} at 310 and 270 nm); however, our

(47) Becke, A. D. *J. Chem. Phys.* **1993**, *98*, 5648−5652.
(48) Svec, H. J.; Junk, G. A. *J. Am. Chem. Soc.* **1967**, *89*, 2836−2840.
(49) Koopmans, T. A. *Physica* **1968**, *1*, 104.

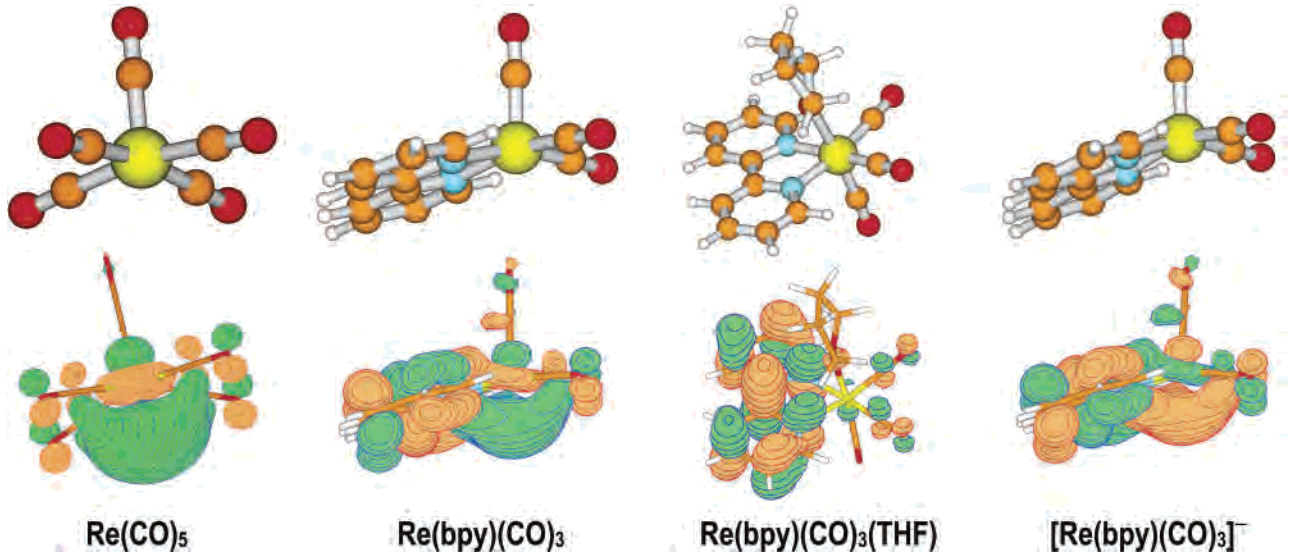

Figure 9. Optimized geometric structures and HOMOs for Re(CO)$_5$, Re(bpy)(CO)$_3$, Re(bpy)(CO)$_3$(THF), and [Re(bpy)(CO)$_3$]$^-$.

assignment of the second absorption (dπ_{MM}* to CO*) is not the same as that previously assigned.[10]

Chemical Properties of the Reduced Re(NN)(CO)$_3$Cl Species. We generated the one-electron reduced species of Re(NN)(CO)$_3$Cl (NN = bpy and dmb) by using Na−Hg in CH_3CN or Na mirror in dry THF.[18] Upon reduction of a yellow solution containing Re(NN)(CO)$_3$Cl in CH_3CN (eq 1), formation of the reddish-purple radical species with the characteristic NN$^{\bullet-}$ absorption around 500 nm was observed. This species is not stable in CH_3CN, and within 1 h, [Re(NN)(CO)$_3$Cl]$^-$ converts thermally to the dinuclear species [Re(NN)(CO)$_3$]$_2$. This change from a reddish-purple solution to a blue-green solution is due to the dimerization of [Re(NN)(CO)$_3$Cl]$^-$ with loss of Cl$^-$ (eqs 10−12 and 7). The dimerization has been observed previously in the electrochemical reduction of Re(NN)(CO)$_3$Cl in CH_3CN and DMF.[30,45,50−53]

$$\mathrm{Re(NN)(CO)_3Cl} + \mathrm{e^-} \rightarrow \mathrm{[Re(NN)(CO)_3Cl]^-} \quad (10)$$

$$\mathrm{[Re(NN)(CO)_3Cl]^-} \rightarrow \mathrm{Re(NN)(CO)_3} + \mathrm{Cl^-} \quad (11)$$

$$\mathrm{Re(NN)(CO)_3} + \mathrm{S} \rightarrow \mathrm{Re(NN)(CO)_3S} \quad (12)$$

However, when THF was used instead of CH_3CN in Na−Hg or Na mirror reduction, we observed the direct formation of the dimer without [Re(NN)(CO)$_3$Cl]$^-$. [Re(NN)(CO)$_3$Cl]$^-$ seems very unstable in THF.

Theoretical Study of Re(bpy)(CO)$_3$Cl and Its One-Electron Reduced Species. In order to understand the properties of [Re(NN)(CO)$_3$Cl]$^-$, we computed the energy at the optimized geometry of Re(bpy)(CO)$_3$Cl, the one-electron reduced Re(bpy)(CO)$_3$Cl$^-$ species, and Re(bpy)(CO)$_3$ formed by loss of Cl$^-$ in the gas phase and in THF solution. The Re−Cl bond energy in the neutral species was found to be 80.9 and 90.2 kcal/mol in the gas phase and in THF solution, respectively. The calculations also show why the singly reduced species leads to formation of the five-coordinate Re(bpy)(CO)$_3$ radical. While the computed reaction energy for the reaction in eq 11 is +16.0 kcal/mol in the gas phase, the solvation energy of the Cl$^-$ anion changes this value to −21.8 kcal/mol in THF. Experimentally, Re(NN)(CO)$_3$Cl$^-$ is unstable in THF, loses Cl$^-$ and converts to the dimer.

The optimized structures (from B3LYP calculations) and HOMO orbitals (from HF calculations) of Re(bpy)(CO)$_3$ and Re(bpy)(CO)$_3$(THF) are shown in Figure 9 together with Re(CO)$_5$ and [Re(bpy)(CO)$_3$]$^-$. In the B3LYP calculated structure of Re(bpy)(CO)$_3$, the coordination geometry of the Re center is a distorted square pyramid with Re−N 2.135 Å, Re−CO$_{ax}$ 1.886 Å, and Re−CO$_{eq}$ 1.929 Å, $\angle$C$_{ax}$−Re−C$_{eq}$ (91.1°) and $\angle$C$_{ax}$−Re−N (104.0°). The MP2 optimized geometry of the Re(bpy)(CO)$_3$ species is in excellent agreement with the B3LYP geometry. The unpaired electron in the 5-coordinate monomer radical is found to occupy a molecular orbital that is partially localized on the metal center and partially delocalized onto the π system of the bpy ring (see Figure 9). The gas-phase five-coordinate monomer radical binds THF by ~18 kcal/mol in the sixth coordination position, and the unpaired electron in the SOMO (singly occupied molecular orbital) can be pushed onto the bpy moiety (where it is already partially delocalized) by an oxygen lone pair from a THF solvent molecule, thereby creating a six-coordinate, 18-electron metal center. The experimental CO stretching frequencies observed for Re(bpy)(CO)$_3$(THF) are 1989 and 1887 (br) cm^{-1}. Our calculated CO stretching frequencies in the gas phase are 1980, 1896, and 1878 cm^{-1} (where the last two frequencies are

(50) Christensen, P.; Hamnett, A.; Muir, A. V. G.; Timney, J. A. *J. Chem. Soc., Dalton Trans.* **1992**, 1455−1463.
(51) Johnson, F. P. A.; George, M. W. W.; Hartl, F.; Turner, J. J. *Organometallics* **1996**, *15*, 3374−3387.
(52) O'Toole, T. R.; Sullivan, B. P.; Meyer, T. J. *J. Am. Chem. Soc.* **1989**, *111*, 5699−5706.
(53) O'Toole, T. R.; Sullivan, B. P.; Bruce, M. R.-M.; Margerum, L. D.; Murray, R. W.; Meyer, T. J. *J. Electroanal. Chem.* **1989**, *259*, 217−239.

merged into one peak with Gaussian line broadening with $\sigma = 4\ cm^{-1}$), in excellent agreement with the experimental results.

Now we consider the equilibrium between $Re(bpy)(CO)_3(THF)$ and $Re(bpy)(CO)_3$ as shown in eq 3. We can estimate the equilibrium constant for the pre-equilibrium in solution by assuming only that differences in the zero-point and thermal energies of the gas-phase species do not change much upon solvation, and using the experimental free energy of vaporization of THF in the following sequence of reactions:

$$[Re^{I}(bpy^{\bullet-})(CO)_3(THF)]_g \rightleftharpoons [Re(bpy)(CO)_3]_g + [THF]_g \qquad \Delta G^\circ = +4.53\ \text{kcal/mol} \quad (13)$$

$$[Re^{I}(bpy^{\bullet-})(CO)_3(THF)]_{solv} \rightleftharpoons [Re^{I}(bpy^{\bullet-})(CO)_3(THF)]_g \qquad \Delta G^\circ = +11.48\ \text{kcal/mol} \quad (14)$$

$$[Re(bpy)(CO)_3]_g \rightleftharpoons [Re(bpy)(CO)_3]_{solv} \qquad \Delta G^\circ = -12.91\ \text{kcal/mol} \quad (15)$$

$$[THF]_g \rightleftharpoons [THF]_{liq} \quad \Delta G^\circ = -\Delta G_{vap}{}^\circ = -0.67\ \text{kcal/mol} \quad (16)$$

$$[Re^{I}(bpy^{\bullet-})(CO)_3(THF)]_{solv} \rightleftharpoons [Re(bpy)(CO)_3]_{solv} + [THF]_{liq} \quad \Delta G^\circ = +2.42\ \text{kcal/mol} \quad (17)$$

Here eq 17 is the sum of eqs 13−16. The free energy in eq 13 was calculated from the gas-phase electronic energies and vibrational frequencies. The gas-phase $Re(bpy)(CO)_3$ monomer is predicted, on the basis of electronic energy with no zero-point energy correction, to bind THF in the sixth coordination site by 18.2 kcal/mol (17.8 with Jaguar). With the inclusion of zero-point energies, this binding energy is reduced to 16.9 kcal/mol. At 298 K, ΔH° for the gas-phase dissociation of $Re^{I}(bpy^{\bullet-})(CO)_3(THF)$ is 16.3 kcal/mol, but owing to a large ΔS°, ΔG° is only 4.5 kcal/mol. The free energies in eqs 14 and 15 were calculated by reoptimizing the geometry in these species in THF solution using the SCRF method implemented in Jaguar 5.0. The free energy of eq 16 was calculated from the NIST tabulated experimental enthalpy and entropy of vaporization of THF.[54] We have carried out a more rigorous, but more complicated, analysis that yields the same result and shows that the computed ΔG° of eq 17 corresponds to the standard state for THF as the pure liquid. The resulting $K_{eq} = [Re(bpy)(CO)_3]/[Re^{I}(bpy^{\bullet-})(CO)_3(THF)]$ for the bond-breaking reaction in THF solution is calculated to be 1.7×10^{-2}. Defining $f = K_{eq}/(1 + K_{eq}) = 1.6 \times 10^{-2}$ to be the fraction of all monomeric species in the form of $Re(bpy)(CO)_3$ after the pre-equilibrium is established, we see that the initial rate of dimerization will be roughly

$$-d[Re]/dt = 2k_2[Re]_0{}^2 f^2 = 2k_2[Re]_0{}^2\ (2.7 \times 10^{-4}) \quad (18)$$

or about 10^{-4} times the rate expected if the solvent did not coordinate at the recombination site. The value of K_{eq} decreases by over an order of magnitude for each kcal/mol of additional binding free energy, so our predicted slowing of the recombination rate is certainly consistent with the observed $\sim 10^{-8}$ effect within the expected accuracy of our calculations, especially as the calculations tend to underestimate binding energies.

Once a THF solvent molecule occupies the sixth coordination site on the Re center of the monomer radical, it becomes a kinetically impeded process for the monomer species to recombine to form the dimer species as shown in eqs 3−5. Even though the calculated Re−Re binding energy of the dimer is 22.4−25.3 kcal/mol in THF solution, larger than the calculated binding energy of Re to THF, the pre-equilibrium with the high concentration of solvent molecules (in excess of Re monomeric species by a factor of $\sim 10^5$) keeps the concentration of five-coordinate monomer species very small. Ultimately, all the monomeric species dimerize, but this happens at a much slower rate than if the solvent did not bind to the five-coordinate monomer radical. It is noteworthy that $Re(CO)_5$, which dimerizes rapidly, is a metal-centered radical that does not bind THF in the sixth coordination position because it cannot form a low-lying π anion radical, and hence cannot achieve an 18-election environment at the metal center.

The Re−Re bond energy for the skewed *cis* conformer calculated with Jaguar in THF solution is 22.4 kcal/mol, and the binding enthalpy of THF in the sixth coordination site, based on the gas-phase zero-point and thermal energies, the solvation energies of the Re monomeric species, and the free energy of vaporization of THF, is 7.2 kcal/mol. This latter value is consistent with the measured activation enthalpy (14 kcal/mol) for the dimerization process in THF solution in the sense that the endothermicity of ligand removal in an S_N1 reaction must be a lower bound on the activation energy.

Theoretical and Experimental Studies of the Doubly Reduced Species $[Re(bpy)(CO)_3]^-$. Further reduction of $[Re(bpy)(CO)_3]_2$ in THF produces the $[Re(bpy)(CO)_3]^-$ anion species which has an absorption maximum at 570 nm, similar to $[Re(dmb)(CO)_3]^-$ reported previously (eq 19).[18]

$$[Re(NN)(CO)_3]_2 + 2e^- \rightarrow 2[Re(bpy)(CO)_3]^- \quad (19)$$

Similar spectral changes from $Re(NN)(CO)_3(OTf)$ to $[Re(NN)(CO)_3]^-$ were observed in CH_3CN. The two-electron-reduced species $[Re(bpy)(CO)_3]^-$ and $[Re(dmb)(CO)_3]^-$ are very stable in dry, air-free THF, despite reports to the contrary. No decomposition of $[Re(NN)(CO)_3]^-$ was observed overnight. However, $[Re(NN)(CO)_3]^-$ is less stable in CH_3CN and converts to an unknown red species in a few days. The UV−vis spectra of $[Re(bpy)(CO)_3]_2$ and $[Re(bpy)(CO)_3]^-$ are shown in Figure 8, along with calculated transition energies and oscillator strengths. Note that while the UV−vis spectra of $[Re(NN)(CO)_3]_2$ are solvent dependent due to the charge-transfer origin of the bands (MLCT), those of $[Re(NN)(CO)_3]^-$ in CH_3CN and THF are remarkably similar.

In the B3LYP calculated structure of $[Re(bpy)(CO)_3]^-$, the coordination geometry of the Re center is a distorted square pyramid with Re−N 2.104 Å, $Re-CO_{ax}$ 1.891 Å, and

(54) NIST Standard Reference Data Program, http://webbook.nist.gov, 2004.

$Re-CO_{eq}$ 1.922 Å, similar to Re(bpy)$(CO)_3$ (Re−N 2.135 Å, $Re-CO_{ax}$ 1.886 Å, and $Re-CO_{eq}$ 1.929 Å). However, $\angle C_{ax}-Re-C_{eq}$ (93.0°) and $\angle C_{ax}-Re-N$ (107.9°) in [Re(bpy)$(CO)_3]^-$ are larger than those (91.1° and 104.0°, respectively) in Re(bpy)$(CO)_3$, indicating that [Re(bpy)$(CO)_3]^-$ has a more distorted square pyramidal geometry.

The time-dependent B3LYP calculations of transition energies predict that the lowest-energy transition is the HOMO (a′) to LUMO (a′) excitation mixed with a substantial HOMO to LUMO + 2 (a′) contribution at 646 nm with an oscillator strength of 0.0524. The HOMO is primarily the metal d_{z^2} orbital with some contributions from the bpy π^* and axial CO σ^* orbitals. The LUMO has mostly bpy π^* character with some metal $d_{x^2-y^2}$ character, and the LUMO + 2 is primarily a bpy* orbital. The next lowest transition is the HOMO to LUMO + 1 (a″) transition at 537 nm with an oscillator strength of 0.0649. The LUMO + 1 is σ^* between the metal and the bpy nitrogen atoms, and between the metal and the equatorial CO ligands, again involving the metal $d_{x^2-y^2}$ orbital. The next transition is primarily the HOMO to LUMO + 2 with a contribution from HOMO to LUMO at 534 with an oscillator strength of 0.1246. Because the metal character of the HOMO is larger than that of the other orbitals involved in these transitions, we may characterize all of these as MLCT transtions. These predicted transitions and relative intensities are in excellent agreement with the experimental UV−vis spectrum, being only slightly shifted to higher energies. The geometric structure of the monomer anion is seen in Figure 9 to be quite similar to that of the monomer radical. Furthermore, the character of the HOMO of the monomer radical is predicted by our calculations not to change significantly upon the addition of an extra electron to form the Re(bpy)$(CO)_3^-$ anion; however, unlike the neutral radical, the anion does not bind THF in the sixth coordination site.

The crystal structure and spectroscopic properties of [Mn(tmbp)$(CO)_3]^-$ and its one-electron energies and percentage composition of selected occupied and unoccupied molecular orbitals calculated by ADF/BP[55,56] have been reported.[46] The coordination geometry of the Mn center is a distorted square pyramid, which is quite similar to the calculated geometry of [Re(bpy)$(CO)_3]^-$. The characters of the HOMO (tmbp π^* + d), LUMO (tmbp π^*), LUMO + 1 (tmbp π^*), and LUMO + 2 (tmbp π^* + d) orbitals of [Mn(tmbp)$(CO)_3]^-$ are slightly different from our calculated orbitals of [Re(bpy)$(CO)_3]^-$, but the delocalized nature of the excess electrons over the tmbp ligand, Mn, and CO moieties found in this complex is similar to that observed in [Re(bpy)$(CO)_3]^-$.

(55) Fonseca Guerra, C.; Snijders, J. G.; te Velde, G.; Baerends, E. J. *Theor. Chem. Acc.* **1998**, *99*, 391−403.
(56) van Gisbergen, S. J. A.; Snijders, J. G.; Baerends, E. J. *Comput. Phys. Commun.* **1999**, *118*, 119−138.

Conclusions

Theory has identified the nature of the monomer species (the five-coordinate metal-centered radical and the six-coordinate ligand π anion radical) involved in the "pre-equilibrium" for dimer formation. As predicted from experimental data, the six-coordinate ligand π radical is more stable than the five-coordinate metal-centered radical, and the estimated fraction of the five-coordinate monomer is 1.6×10^{-2} and would decrease by over an order of magnitude for each additional kcal/mol of THF binding free energy. Theory has also identified the favored geometrical structure of the dimer, which is the skewed *cis* conformer (rotated 52° about the Re−Re bond from the *cis* configuration in the MP2 optimized structure) in which there is no low-lying unoccupied Re−Re orbital that is σ_{MM}^* in character. It has explained why [Re(bpy)$(CO)_3$Cl]$^-$ spontaneously forms Re(bpy)$(CO)_3$(THF) in THF solution, and why the dimerization reaction is strikingly slow compared to that of $Re(CO)_5$. The extremely slow dimerization arises from the solvent blocking the binding site, which is consistent with experimental observations. The dimerization process proceeds via the Re-centered radical that is involved in an unfavorable pre-equilibrium. Our finding demonstrates that the reactivity of a metal center (in the present case the Re dimerization reaction) depends on the electron population on the metal center and can be manipulated by the choice of solvent or ligands. Finally, theory has elucidated the nature of the excited electronic states in the UV−vis spectra of the dimer and monomer anion.

Acknowledgment. We thank Drs. Norman Sutin, Sergei Lymar, Carol Creutz, and Bruce S. Brunschwig for valuable discussions. This work was performed at Brookhaven National Laboratory, funded under Contract DE-AC02-98CH10886 with the U.S. Department of Energy and supported by its Division of Chemical Sciences, Office of Basic Energy Sciences.

Supporting Information Available: Additional tables and figures. This material is available free of charge via the Internet at http://pubs.acs.org.

IC048910V